A Deep Insight into the Photoluminescence Properties of Schiff Base Cd(II) and Zn(II) Complexes

Inorganic Chemistry

Article

Cite This: Inorg. Chem. XXXX, XXX, XXX-XXX

pubs.acs.org/IC

A Deep Insight into the Photoluminescence Properties of Schiff Base Cd^{II} and Zn^{II} Complexes

Ishani Majumder,[†] Prateeti Chakraborty,*[,‡] Sanchari Dasgupta,[†] Chiara Massera,[§] Daniel Escudero,*[,Δ] and Debasis Das*[,†]

[†]Department of Chemistry, University of Calcutta, 92 A. P. C. Road, Kolkata 700009, India

[‡]Department of Chemistry, Bangabasi College, 19, Rajkumar Chakraborty Sarani, Kolkata 700009, India

[§]Dipartimento di Scienze Chimiche, della Vita e della Sostenibilità Ambientale, University of Parma, Viale delle Scienze 17/A, 43124 Parma, Italy

[Δ]Chimie Et Interdisciplinarité, Synthèse, Analyse, Modélisation, BP 92208, UMR CNRS No. 6320, Université de Nantes, 2, Rue de la Houssinière, 44322 Nantes, Cedex 3, France

Supporting Information

ABSTRACT: A tridentate N,N,O donor ligand 2,4-dichloro-2-[(2-piperazine-4-yl-ethylimino)-methyl]-phenol (HL) was designed, and eight new Zn^{II} and Cd^{II} complexes, namely, $[Zn(LH)(SCN)_2]$ (**1**), $[Zn(LH)(N_3)_2]$ (**2**), $[Zn(LH)(NO_2)_2]$ (**3**), [Zn(LH)(dca)(OAc)] (**4**), $[Cd_2(LH)_2(SCN)_4]$ (**5**), $[Cd(LH)(N_3)_2]$ (**6**), $[Cd(LH)(NO_2)_2]$ (**7**), and [Cd(LH)(dca)(OAc)] (**8**) [where dca = dicyanamide anion] were synthesized. Five of them (**1**, **2**, **4**, **5**, **7**) were structurally characterized through single-crystal X-ray diffraction analysis. H-Bonding interactions are found to be the major stabilizing factor for crystallization in the solid state. Experimental and computational studies were performed in cooperation to provide a rationalization of the photoluminescence properties of those complexes. The quantum yields are anion-dependent, with enhanced efficiencies in the following order: LH < Cd-SCN(**5**) < Cd-dca(**8**) < Cd−N_3(**6**) < Cd-NO_2(**7**) < Zn-dca(**4**) < Zn−N_3(**2**) < $ZnNO_2$(**3**) < ZnSCN(**1**). By using quantum chemical calculations we rationalized the above trends. Moreover, the diverse lifetimes observed for those eight complexes were also quantitatively explained by considering the subtle competition between different photo-deactivation pathways.

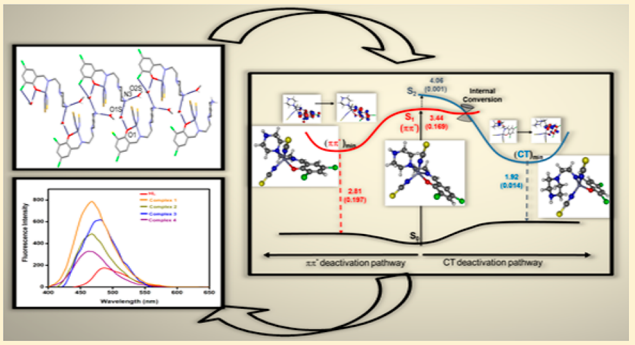

INTRODUCTION

Schiff bases are important scaffolds in coordination chemistry, with a broad range of multidisciplinary applications, for example, as precious catalysts,[1−3] pharmaceutical agents,[4,5] and in everyday chemistry applications like food industry, dye industry, and many more.[6,7] The complexes derived from these Schiff base ligands are considered to be among the most important stereochemical models in main group and transition metal coordination chemistry due to their biodegradability, cheap and easy production, and their adequate electrical conductivity in conjugated compounds. Schiff base complexes are also of increasing interest in photonic applications.[8] More particularly in the field of optoelectronics, luminescent 4f and polynuclear 4f-3d Schiff base complexes have been extensively explored.[9] Several strategies to enhance their photoluminescent properties have been envisaged. Schiff base complexes of d^{10} metal ions, for example, Zn^{II}, Cd^{II}, and Hg^{II}, usually exhibit enhanced photoluminescent properties as compared to their free ligands.[10] These complexes may typically exhibit ligand-centered (LC)- or ligand-to-ligand charge transfer (LLCT)-based photophysics. Their enhanced photoluminescent properties usually root on the chelation-induced fluorescent enhancement effect,[11−14] namely, the quench of nonradiative decay in the more rigid Schiff base complexes. Besides the use of these complexes in electrooptical devices, there is an increasing interest for their biological and environmental applications, as Schiff base complexes can be used as selective fluorescent probes for the detection of Zn^{II}, Cd^{II}, and Hg^{II}.[15−17] The recent improvements in computational photochemistry have extended the applications from a qualitative assignment of the emission processes to quantitative interpretation of both emission spectroscopy and photoreactivity.[18] Therefore, this led us to establish the correlation between qualitative and quantitative consequences in the present work. In this contribution we prepared eight new complexes of Zn^{II} and Cd^{II} derived from an N, N, O donor Schiff base ligand. Furthermore, we quantitatively determined for the first time the photoluminescence quantum yields of Schiff base complexes from first principles. These complexes possess intricate photo-

Received: July 3, 2017

DOI: 10.1021/acs.inorgchem.7b01692
Inorg. Chem. XXXX, XXX, XXX−XXX

Scheme 1. Synthetic Route of the Complexes

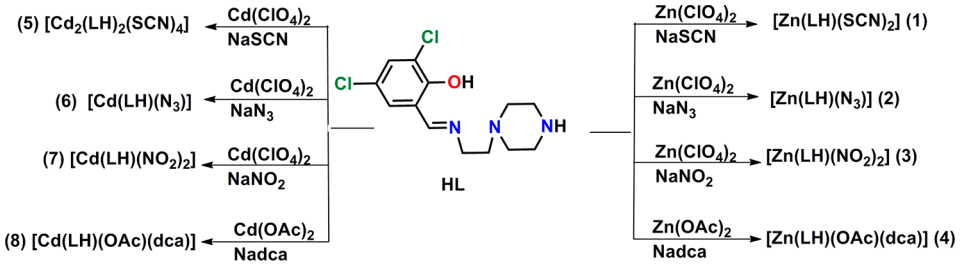

deactivation dynamics, as reflected by the time-resolved experiments and the computational investigations.

EXPERIMENTAL AND COMPUTATIONAL DETAILS

Experimental Details. 3,5-Dichlorosalicylaldehyde and *N*-(2-aminoethyl)piperazine were purchased from Sigma-Aldrich. The other organic reagents and solvents used in this project were of analytical reagent grade and purchased from marketable suppliers. The solvents used in the experiments were redistilled before use. Water used in all physical measurements and experiments was Milli-Q grade. A PerkinElmer 240C analyzer was used to perform the elemental analyses (C, H, N). Shimadzu FTIR-8400S and PerkinElmer Spectrum Express Version 1.03 were used for recording infrared spectra (4000−400 cm^{-1}) at 28 °C using KBr pellets as medium. A Shimadzu UV-2450PC spectrophotometer equipped with multiple cell-holders and thermostat was used to monitor the UV−visible spectra. A Hitachi model F-7000 spectrofluorimeter equipped with a150 W xenon lamp was used to measure the steady-state emission at 298 K using a stoppered cell of 1 cm path length. A Horiba Jobin Yvon Fluorocube-01-NL was used to perform the fluorescence lifetime measurement study.

The fluorescence quantum yield (Φ) of each complex was evaluated by comparing the corrected emission spectra of the complexes with that of the anthracene measured in methanol (Φ = 0.20)[19] considering the total area under the emission curve. The solvent correction was done according to eq 1[20]

$$\Phi_S = \Phi_R \frac{F_S}{F_R} \frac{OD_R}{OD} \frac{\eta^2}{\eta_R^2} \quad (1)$$

where Φ is the quantum yield of the compounds, *F* is the integrated fluorescence intensity (area under the emission curve), OD is the optical density, and η is the refractive index of the medium. It is assumed that all the complexes and the reference are excited at the same wavelengths of 385 and 412 nm. The subscript R refers to the reference fluorophore (anthracene in this case) of known quantum yield. The standard quantum yield value was then used for the calculation of the radiative and nonradiative rate constants.

Singlet-state lifetimes were measured using a Time Master fluorimeter from Photon Technology International (PTI, USA). The system consists of a pulsed laser driver PDL-800-B (from Pico-Quant, Germany) with interchangeable sub-nanosecond pulsed LEDs and pico-diode lasers (PicoQuant, Germany) with a TCSPC setup (PTI, USA). The lifetimes of the complexes were measured by using diode lasers LDH-375 (pulse width 200 ps), Germany, at a repetition frequency of 4 MHz. Instrument response functions (IRF) were measured at the excitation wavelength of 375 nm (in the case of a diode laser) using slits with a band-pass of ∼1−3 nm using Ludox silica as scatterer. Intensity decay curves were fitted as a summation of exponential terms.

$$F(t) = \sum \alpha_i \exp(-t/I')_i \quad (2)$$

The decay parameters were recovered using a nonlinear iterative fitting procedure based on the Marquardt algorithm.[21] A deconvolution technique was used to determine the lifetime up to 150−200 ps with the light-emitting diode (LED), while the time resolution was 100 ps with the diode laser. The quality of the fit was assessed over the entire decay, including the rising edge, and tested with a plot of weighted residuals and other statistical parameters, for example, the reduced χ^2 ratio and the Durbin−Watson (DW) parameters.[22] Detailed description of the synthesis of the complexes are presented in the Supporting Information.

Computational Details. Ground-state geometry optimizations and analytical frequency calculations were performed with density functional theory (DFT; PBE0).[23,24] Excited-state geometry optimizations and numerical frequency calculations were performed with time-dependent (TD) DFT. PBE0 is also used in the TD-DFT calculations, since this functional is found to provide a good balance between local excited (LE) and intramolecular charge transfer (CT) states, with average absolute errors of ca. 0.14 eV for the low-lying excited states of conjugated organic compounds.[25] The 6-31G* basis sets were used for all atoms, and the MWB28 pseudo potential was used for the Cd^{II} atoms. Both the DFT and TD-DFT calculations were performed in the presence of dimethyl sulfoxide (DMSO) implicitly using the polarizable continuum model (PCM). All the calculations were performed with the Gaussian09[26] program package. In the case of complex **5**, a monomeric model was used (i.e., $[Cd(LH)(SCN)_2]$). For the rate calculations of complex **7** the MOMAP suite of programs was used.[27] The radiative and nonradiative rates are evaluated by using the thermal vibration correlation function (TVCF) theory. For the rate calculations, the difference between two electronic state PESs was considered by using $\underline{Q}_e = S\cdot\underline{Q}_g + \underline{D}_e$, where *S* is the Duschinsky rotation matrix, $\underline{Q}_e$ and $\underline{Q}_g$ are the normal-mode coordinates of the ground and excited states, respectively, and $\underline{D}_e$ is the displacement between the minima of the excited- and ground-state geometries. First-order perturbation theory was applied to compute the nonadiabatic electronic coupling, which required the evaluation of the transition electric field. Herein, the transition electric field (see eq 41 in ref 28) was evaluated at the TD-PBE0/6-31G* level of theory with the Gaussian09 package. The derivatives of the transition dipole moments were calculated numerically around the equilibrium geometry of the ground state at the PCM-TD-PBE0/6-31G*. More details on the TVCF formalism to obtain the radiative and nonradiative decay rates can be found in the Supporting Information and ref 27.

RESULTS AND DISCUSSION

Synthesis, Rationalization, and Characterization of the Metal Complexes. Eight complexes (**1**−**8**) were prepared by adopting template synthetic procedure, where perchlorate or acetate salts of zinc(II) and cadmium(II) along with four coligands (SCN^-, N_3^-, NO_2^-, and $N(CN)_2^-$) were added to the Schiff base {2-(2-piperzine-1-yl)ethylimino)methyl)-4,6-dichlorophenol} formed in situ via condensation between the aldehyde and the amine (Scheme 1). All the complexes except **3**, **6**, and **8** were structurally characterized by X-ray single-crystal structural analyses.

IR and UV−Vis Spectra of the Complexes. Figures S1−S8 in the Supporting Information show the IR spectra of the eight complexes. All the complexes show a sharp band due to a C═N stretching in the region of 1630−1650 cm^{-1} and also a band around 1440−1450 cm^{-1} due to skeletal vibrations. The

DOI: 10.1021/acs.inorgchem.7b01692
Inorg. Chem. XXXX, XXX, XXX−XXX

appearance of a broad band around 2079 cm^{-1} indicates the presence of a coordinated thiocyanate anion in **1**, but in **5** the broad band is bifurcated at 2031 and 2113 cm^{-1} indicating the ambidentate nature of the coordinated thiocyanate anion in the complex. Bands around 2065 and 2053 cm^{-1} confirm the presence of non-coordinated azide in complexes **2** and **6**, respectively. A peak around 1415 cm^{-1} appears due to the presence of a coordinated nitrite anion in complexes **3** and **7**, respectively. In complexes **4** and **8** peaks due to coordinated acetate and the dicyanamide (dca) anions appear in the regions of 1139, 2170 cm^{-1} and 1322, 2157 cm^{-1}, respectively. The absorption spectra of all the complexes were measured in DMSO, and they are presented in Figure S9 (for zinc complexes) and Figure S10 (for cadmium complexes). All the complexes, regardless of the metal ion, show a lower energy band around 385 nm (412 nm for **3**), which is due to n→π^* transitions and a band around 258 nm due to $\pi\rightarrow\pi^*$ transitions. The presence of similar absorption peaks shown by all the complexes indicates similar structural features in solution.

Solution Studies: Mass Spectrometry. To rationalize the solution-state composition of the complexes, electrospray ionization−mass spectrometry (ESI-MS) studies were performed in DMSO−MeCN medium (Figures S11−S26). The spectral analysis reveals that a similar type of soft ionization happens in the complex solutions. Complexes **1**−**3** show a sharp peak at around *m*/*z* 365.99 amu due to the formation of a $[Zn(L)]^+$ monocation. Another small peak at around 302.07 amu appears due to the ionization of the free ligand. Interestingly, complex **4** dissociates slightly differently from the rest of the series having one dicyanamide anion attached with the $[Zn(L)]^+$ group, along with the protonation of the piperazine amine group. The observed peak for $[Zn(L)(dca)]^+$ is 433.0253 amu, and the calculated peak is 433.0103 amu. Complex **5**, a dinuclear Cd complex, dissociates to a monouclear complex and ionizes as the $[Cd(L)]^+$ monocation, with an observed peak at 413.9862 amu (calcd 413.9700 amu). Complexes **6** and **7** dissociate and ionize similarly to give the base peak at 413.9696 and 413.9821 amu, respectively, thus corroborating the presence of a $[Cd(L)]^+$ monocation. Again the Cd-dca complex undergoes dissociation and ionization similar to its analogous zinc complex. The base peak that appears corresponds to the $[Zn(L)(dca)]^+$ cation, with an observed 480.9897 amu (calcd 480.9870 amu).

Crystal Structure Description of the Complexes. X-ray diffraction analysis on single crystals revealed that in the solid state all the compounds contain the ligand LH in a zwitterionic form, since the phenolato oxygen atom is deprotonated and a nitrogen atom in the piperazine unit is protonated.

*Complex [Zn(LH)(SCN)$_2$] (**1**).* Compound **1** is the mononuclear complex $[Zn(LH)(NCS)_2]\cdot 2CH_3OH$. The molecular structure of $[Zn(LH)(SCN)_2]$ (**1**) is shown in Figure 1, and selected bond lengths and angles are listed in Table S3. The metal center is tetracoordinated in a distorted tetrahedral environment. The ligand shows a chelating behavior through the phenolato oxygen atom O1 and the iminic nitrogen atom N1, while the two remaining positions are occupied by thiocyanate ions, which ensure the neutrality of the complex. The ethylpiperazine arm is bent so that the lone pair of the N2 atom points toward the zinc ion. The complexes are connected through a network of methanol-mediated H bonds (see Figure 2).

*Complex [Zn(LH)(N$_3$)$_2$] (**2**).* Compound **2** is the monomeric complex $[Zn(LH)(N_3)_2]$, in which the Zn ion shows a five-coordinated geometry (Figure 3). The ligand behaves in a tridentate fashion (unlike compound **1**) with the atoms O1 and N2 at the vertices of a regular trigonal bipyramid. The equatorial positions are occupied by N1 from LH and by two nitrogen atoms N4 and N7 belonging to two azido ions. The usual zigzag supramolecular chain is formed by adjacent molecules, which are held together by hydrogen bonds between the protonated $-NH_2^+$ from the piperazine unit and the phenoxide oxygen O1 (see Figure 4).

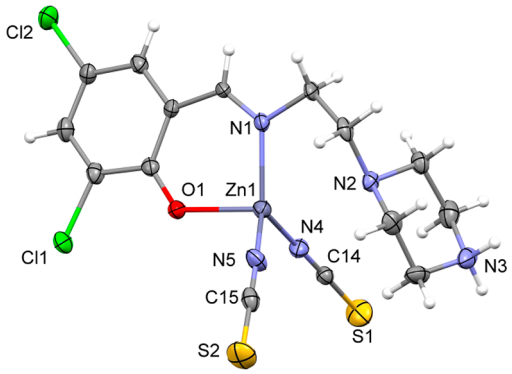

Figure 1. Ortep view (20% probability level) of **1** with partial labeling scheme. Lattice methanol molecules are not shown.

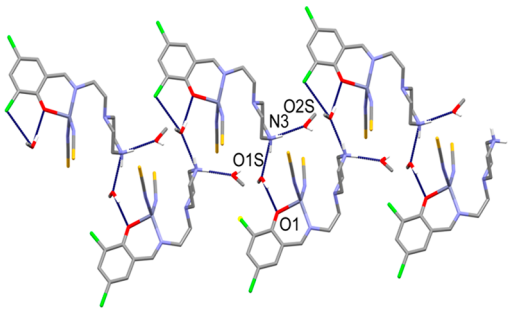

Figure 2. Hydrogen-bond network formed in the crystal structure of **1**. Only the H atoms involved in the interactions (blue lines) are shown.

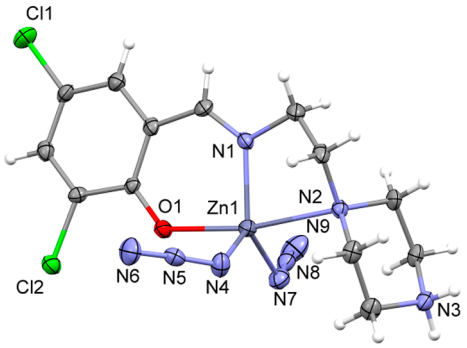

Figure 3. Perspective view (20% probability level) of **2** with partial labeling scheme.

*Complex [Zn(LH)(dca)(OAc)] (**4**).* The structure of complex **4** is similar to that of complex **1** and has the general formula $[Zn(LH)(N_3C_2)(CH_3COO)]$ (Figure 5). The ligand is bidentate through O1 and N1, while N2 does not take part in the coordination, albeit its lone pair points toward the metal center; the zinc ion is therefore tetra-coordinated with one

DOI: 10.1021/acs.inorgchem.7b01692
Inorg. Chem. XXXX, XXX, XXX−XXX

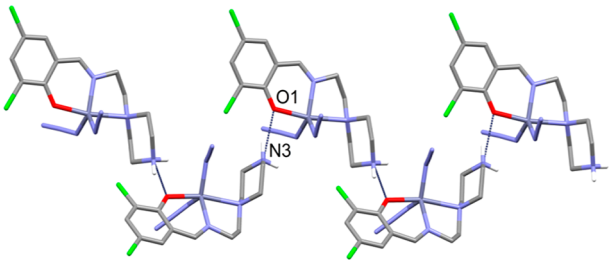

Figure 4. Hydrogen-bond network formed in the crystal structure of **2**. Only the H atoms involved in the interactions (blue lines) are shown.

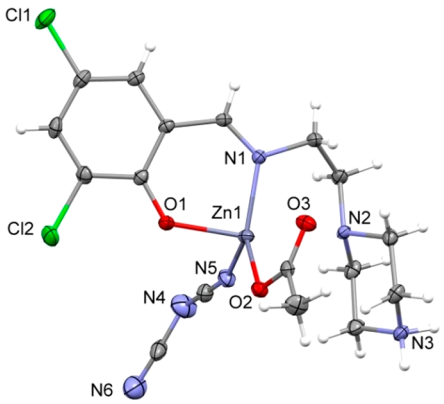

Figure 5. Perspective view (20% probability level) of **4** with partial labeling scheme.

dicyanamide and one acetate ion, which completes the coordination sphere.

The presence of O1 and O2 in a convenient adjacent position allows the formation of a series of bifurcated H bonds with the two hydrogen atoms of the piperazine nitrogen N3, resulting in the usual zigzag motif depicted in Figure 6.

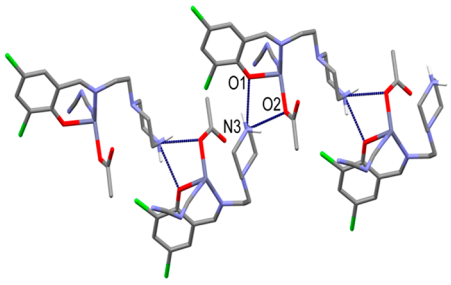

Figure 6. Hydrogen-bond network formed in the crystal structure of **4**. Only the H atoms involved in the interactions (blue lines) are shown.

*Complex $[Cd_2(LH)_2(SCN)_4]$ (**5**).* Compound **5** is the dimeric complex $[Cd_2(LH)_2(SCN)_4]\cdot 2CH_3OH$, in which both cadmium ions show the same octahedral geometric environment of the type N_4OS (Figure 7). Each LH behaves as a tridentate ligand through the oxygen atoms O1A, the iminic nitrogen atom N1A and the piperazine nitrogen atom N2A around Cd1, and the corresponding O1B, N1B, and N2B around Cd2 (see Figure 7). The coordination around each metal center is completed by three thiocyanate ions; one of them is monodentate through its nitrogen atom (N4A or N4B), while the other two are bridging the cadmium ions via the sulfur and nitrogen atoms (N5A, N5B, S2A, and S2B). Also in this case the crystal structure is stabilized by a network of

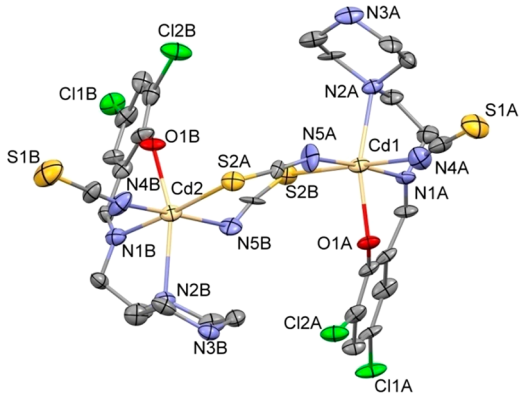

Figure 7. Perspective view (20% probability level) of **5** with partial labeling scheme. Hydrogen atoms and methanol lattice molecules were omitted for clarity.

hydrogen bonds involving the protonated nitrogen atoms N3A and N3B, the phenoxide oxygens O1A and O1B, and the nitrogen atom N4A of one dangling thiocyanate ion (see Figure 8).

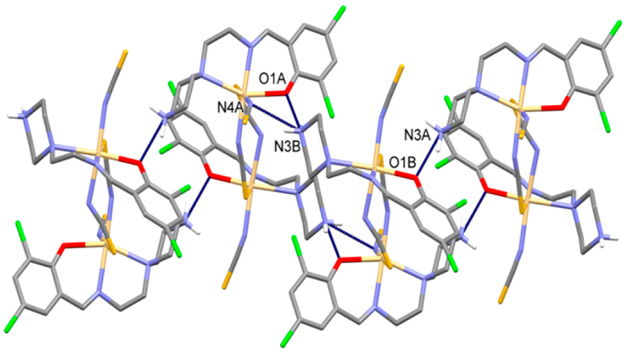

Figure 8. Hydrogen-bond network formed in the crystal structure of **5**. Only the H atoms involved in the interactions (blue lines) are shown. Lattice methanol molecules were omitted for clarity.

*Complex $[Cd(LH)(NO_2)_2]$ (**7**).* Compound **7** is the complex $[Cd(LH)(NO_2)_2]$, in which the coordinating behavior of the ligand is analogous to compound **2**. The presence of two bridging nitrito ions, however, causes the cadmium ion to be seven-coordinated, thus showing a pentagonal bipyramidal geometry. The axial positions are occupied by O1 and N2 from the ligand, while the equatorial positions are occupied by the iminic nitrogen atom N1 and the four oxygen atoms O2, O3, O4, and O5 from the nitrito counterions (see Figure 9). The

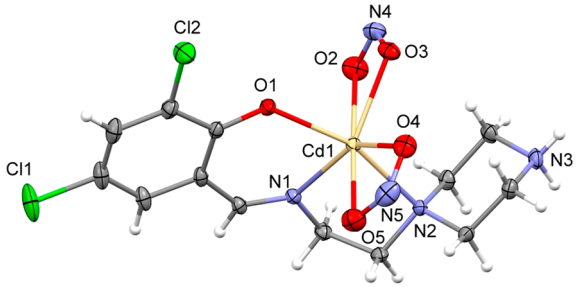

Figure 9. Perspective view (20% probability level) of **7** with partial labeling scheme.

DOI: 10.1021/acs.inorgchem.7b01692
Inorg. Chem. XXXX, XXX, XXX−XXX

network of H bonds is shown in Figure 10, highlighting the typical zigzag pattern that is present in almost all the complexes

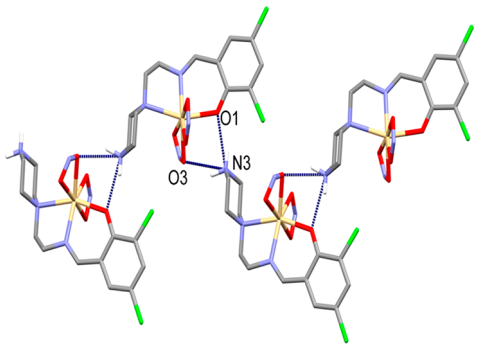

Figure 10. Hydrogen-bond network formed in the crystal structure of 7. Only the H atoms involved in the interactions (blue lines) are shown.

of the series, due to the presence of $-NH_2^+$ as H-bond donor. The H-bond acceptors in this case are the phenoxide oxygen atoms O1 and the nitrito oxygen atoms O3.

3.5. Steady-State and Time-Resolved Emission Spectra. The fluorescence spectra of the eight complexes were measured in DMSO at room temperature (298 K), and they are shown in Figure 11. The emission band's maxima and their relative fluorescence quantum yields are provided in Table S8. In each case the ligand LH shows the lowest quantum efficiency, as usually explainable from the free rotation of ligand. After complexation, there is a ca. 8−10-fold (5−6-fold) increase of the quantum efficiency in the Zn (Cd) complexes. The increase of fluoresce intensity on zinc complexes over cadmium complexes is presumably due to heavy atom perturbation effect.[29−31] For this series, the fluorescence efficiencies are found to be anion-dependent. Thus, the quantum yield of the eight complexes follow the order of LH < Cd-SCN(**5**) < Cd-dca(**8**) < Cd−N_3(**6**) < Cd-NO_2(**7**) < Zn-dca(**4**) < ZnN_3(**2**) < $ZnNO_2$(**3**) < ZnSCN(**1**). The anions (dca^-, N_3^-, NO_2^-) follow similar trends in both the Zn and Cd series. Quantitative rationalizations of the fluorescence trends were established on the basis of theoretical investigations, which are discussed later.

The fluorescence decay lifetimes of the ligand and complexes are shown in Figure 12 with λ_{exc} = 385 nm (412 nm for **3**). Complexes **1**, **3**, and **4** display biexponential decays, while the other complexes require multiexponential decay fits (Table 1). The biexponential decay lifetimes observed for complexes **1**, **3**, and **4** agree well with competition between different excited states, that is, the $\pi-\pi^*$ excited state, involved in the emission features of the complexes, and a dark state of CT character that quenches fluorescence. The multiexponential decay lifetimes indicate population of further CT states along with the main emissive $\pi\pi^*$ state. As observed from the fluorescence study the free ligand exhibits the lowest average lifetime and the lowest quantum yield.

Interpretation of the Fluorescence Properties: Computational Studies. In Figure 13 the potential energy profiles for all possible photo-deactivation pathways of the Zn-thiocyanate (**1**) complex are schematically represented. Vertical emission and absorption energies, along with their oscillator strengths, are also included. The bright state of **1** is S_1 and corresponds to a $\pi\pi^*$ excitation mainly involving the aromatic moiety (see the orbitals involved in Figure 13 (left)). Slightly above in energy is found S_2. This state is a CT state and involves the lone pair of the amino group of the piperazine unit and the aromatic moiety (see the orbitals in Figure 13 (right)). It is characterized by almost negligible oscillator strength, and thus, it is not populated upon experimental irradiation. At the ground-state geometry, the Zn atom displays a pseudotrigonal bipyramidal arrangement, and the aromatic ring is mainly coplanar to the Schiff base. The pseudotrigonal bipyramidal environment is maintained at the optimal $(\pi\pi^*)_{min}$ geometry, but the aromatic ring is tilted with respect to the Schiff base. Conversely, at the optimal $(CT)_{min}$ geometry, the Zn atom adopts a pseudo-octahedral disposition, because of the dechelation of the piperazine unit (see Figure 13 (right)). Importantly, at the optimal $(CT)_{min}$ geometry, the CT state becomes the lowest excited state (it is located below in energy with respect to the $\pi\pi^*$ state). Therefore, as highlighted in Figure 13, the well of the CT state might be populated after internal conversion from the $\pi\pi^*$state. This photo-deactivation pathway is in competition with the straightforward population of the $\pi\pi^*$ well. Fluorescence emission is clearly favorable at the $\pi\pi^*$ well, due to its large oscillator strength (f = 0.197) and the small geometrical relaxation effects with respect to the Franck−Condon region. Conversely, the radiationless deactivation to the ground state is much preferred over the radiative deactivation at the CT well, since this state is characterized by an almost negligible oscillator strength (f = 0.014) and

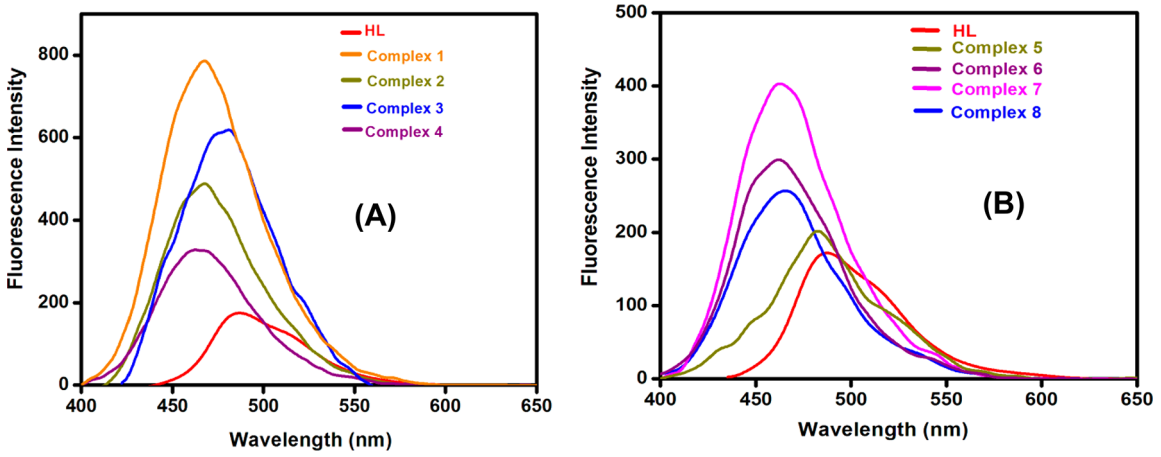

Figure 11. Fluorescence spectra of ligand LH and (A) Zn complexes (**1**−**4**) and (B) Cd complexes (**5**−**8**) in DMSO at298 K; λ_{ex} = 385 nm;.

DOI: 10.1021/acs.inorgchem.7b01692
Inorg. Chem. XXXX, XXX, XXX−XXX

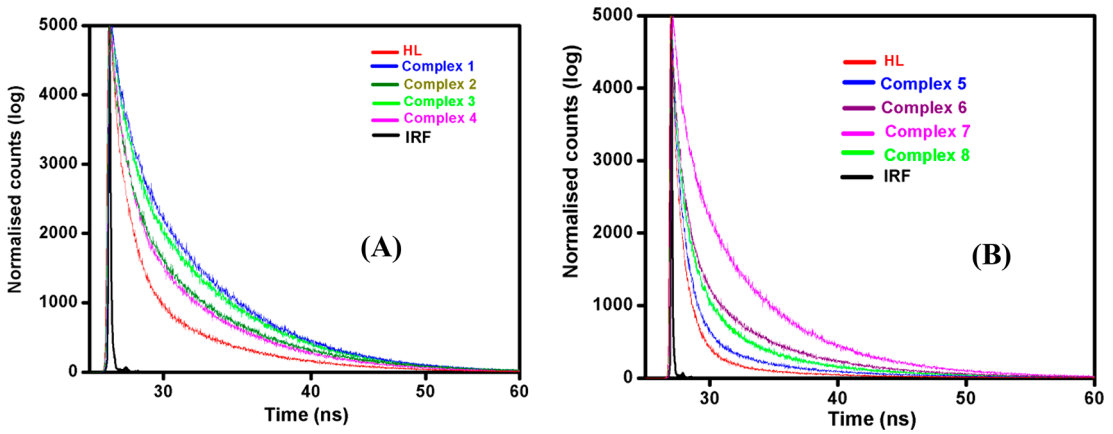

Figure 12. Fluorescence decay of the complexes **1**−**4** (**A**) and **5**−**8** (**B**) in DMSO at 298 K; λ_{exc} for **1**, **2**, **4**, **5**−**8** = 385 nm and λ_{exc} for **3** = 412 nm.

Table 1. Fluorescence and Time-Resolved Emission Data for Ligand and Complexes 1−8 at 298 K at DMSO Medium

ligand/ complex	excitation wavelength (nm)	emission wavelength (nm)	lifetime (ns)			avg lifetime (ns)	relative abundance (α)			χ^2
			I'_1	I'_2	I'_3	$\langle I' \rangle$	α_1	α_2	α_3	
HL	424	485	0.581 365	2.325 46		0.9265	(80.21%)	(19.79%)		1.07
complex **1**	385	466	3.042 606	12.170 43		4.1573	(43.51%)	(56.49%)		0.97
complex **2**	385	468	3.153 905	6.307 81	12.615 62	3.1106	(33.44%)	(9.82%)	(56.74%)	1.16
complex **3**	412	477	2.973 933	11.895 73		3.8560	(48.64%)	(21.36%)		0.97
complex **4**	385	464	2.689 14	10.756 56		2.3855	(64.55%)	(35.45%)		1.01
complex **5**	385	465	1.509 992	8.611 18	4.960 015	1.0797	(33.14%)	(3.03%)	(63.83%)	0.98
complex **6**	385	461	2.453 906	4.907 811	9.815 623	2.0190	(33.98%)	(12.24%)	(53.78%)	1.01
complex **7**	385	462	2.731 985	5.463 969	10.927 94	2.4644	(17.92%)	(18.47%)	(63.61%)	0.97
complex **8**	385	484	2.119 745	4.239 491	8.478 981	1.5254	(17.12%)	(5.68%)	(77.20%)	0.99

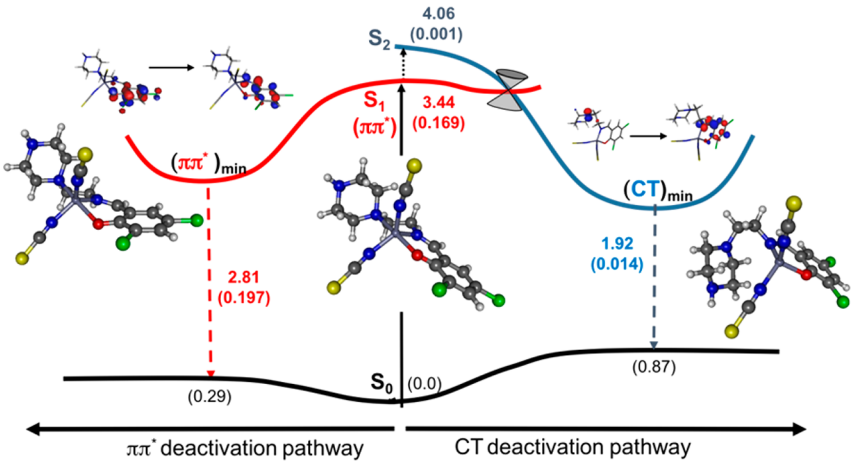

Figure 13. Schematic potential energy profiles (PCM-TD-PBE0/6-31G*) for the $\pi\pi^*$and CT deactivation pathways of the Zn-Thiocyanate complex (**1**). Relative S_0 energies (between parentheses) and emission energies (in eV). Oscillator strengths are given between parentheses.

important geometrical relaxation effects occur along this photodeactivation pathway. This computational evidence is in agreement with the observance of biexponential (for complexes **1**, **3**−**4**) or multiexponential (**2**, **5**−**8**) decay lifetimes. Hence, as shown for complex **1**, the biexponential decay is due to the population of different excited states. Note that these CT states are generally found above the $\pi\pi^*$state at the Franck−Condon region for all the complexes (see Table 2). In Table 2 are summarized the computed absorption and emission properties of selected complexes, namely, the Zn-thiocyanate complex (**1**), the Zn-dicyanamide complex (**4**), the Cd-thiocyanate complex (**5**), the Cd-azide complex (**6**), and the Cd-nitrite complex (**7**). The computed absorption and emission energies are generally in good agreement with the experimental counterparts (see Tables 1 and 2), and the observed trends are recovered by the PCM-TD-PBE0 calculations.

The prediction of the fluorescence quantum efficiencies for compounds **1**−**8** from first principles requires the evaluation of the radiative decay rates arising from the emissive $\pi\pi^*$ state and the sum of all positive nonradiative decay contributions. The prediction of these photophysical properties is still relatively demanding and intricate from a computational viewpoint for these Schiff base complexes, due to the relatively large size of the molecules and their complicated excited-state potential

DOI: 10.1021/acs.inorgchem.7b01692
Inorg. Chem. XXXX, XXX, XXX−XXX

Table 2. Computed Absorption and Emission Maxima (nm) along with Oscillator Strengths (a.u.) for Complexes 1, 4, 5, 6, and 7 at the PCM-TD-PBE0/6-31G* l Level of Theory[a]

complex		absorption energies (oscillator strength)	emission energies (oscillator strength)	k_r (s^{-1})[b]	Φ_{fluo} (%)[c]	reorganization energies λ (cm^{-1})
1	S_1 ($\pi\pi^*$)	360 (0.169)	442 (0.197)	6.7×10^7	0.280 (0.178)	2577
	S_2 (CT)	305 (0.001)				
4	S_1 ($\pi\pi^*$)	356 (0.170)	426 (0.219)	8.1×10^7	0.192 (0.107)	2308
	S_2 (CT)	307 (0.001)				
5	S_1 ($\pi\pi^*$)	355 (0.177)	436 (0.198)	7.0×10^7	0.075 (0.033)	2617
	S_2 (CT)	300 (0.001)				
6	S_1 ($\pi\pi^*$)	356 (0.163)	433 (0.214)	7.6×10^7	0.154 (0.080)	2498
	S_2 (CT)	320 (0.003)				
7	S_1 ($\pi\pi^*$)	354 (0.155)	431 (0.201)	7.3×10^7 (1.2×10^8)	0.178/0.030[d] (0.106)	2523/*2771*[d]
	S_2 (CT)	333 (0.007)				

[a]Computed radiative rates, fluorescence quantum yields, and reorganization energies for all the complexes are also included. [b]Value between parentheses corresponds to the one obtained with the TVCF formalism. [c]Values between parentheses correspond to the experimental values. [d]Values in italics corresponds to the ones obtained with the TVCF formalism.

energy surface (PES; see the Discussion for **1** above). Hence, the direct comparison with the experimental results may become a difficult task due to the multiply competing deactivation processes. Herein, the radiative rates from the emissive $\pi\pi^*$ state for all the complexes were evaluated using Einstein spontaneous emission formula

$$k_r = 0.67 f E_{em}^{\ 2} \quad (3)$$

where the emission energy (in wave numbers) and its associated oscillator strength (f_i) are computed at the PCM-TD-PBE0/6-31G* level of theory. These values are reported in Table 2. The fluorescence quantum yields for all the complexes were estimated using

$$\Phi_{fluo} = k_r/(k_r + \sum k_{nr}) = k_r I' \quad (4)$$

where $\sum k_{nr}$ stands for all possible nonradiative decay channels depopulating the emissive $\pi\pi^*$state, and I' stands for the average decay lifetime. Because of the difficulty to assign from a computational viewpoint all possible nonradiative channels, herein we use the experimental I' values tabulated in Table 1 to estimate the Φ_{fluo} values according to eq 4. The reorganization energies (λ) can be approximated as half of the Stokes shift. The computed λ values are also reported in Table 2. For all complexes, their computed Φ_{fluo} values are systematically larger than their experimental counterparts. Importantly, the experimental trend in the Φ_{fluo} values is fully recovered by our calculations. Since similar (i) radiative rates and (ii) reorganization energies are obtained for all the complexes, the main factor determining their Φ_{fluo} values is the I' value. For complexes **5**−**7**, the population of multiple nonradiative channels competing to the radiative decay, that is, dark-state quenching (see above)[32] and intersystem crossing (ISC) processes, in a greater extent than for complexes **1**, **4**, which experimentally show a biexponential decay, leads to their observed decreased I' values and consequently to an enhanced quench of fluorescence. Certainly, as we stated in the introduction, the Cd complexes are more prone to ISC than the Zn ones, and that might partially explain these differences. Additionally, for **7**, we use herein the TVCF formalism to compute the radiative and nonradiative decay rates arising from the emissive $\pi\pi^*$state.[33] This formalism uses a multidimensional harmonic oscillator model coupled with DFT and TD-DFT calculations, where displacements, distortions, and Duschinsky rotations are considered (see the Computational Details). This strategy has proven successful for predicting fluorescence properties of organic and organometallic polyatomic systems.[34,35] Neglecting the contribution of the dark and triplet states to the global efficiencies, the fluorescence quantum yields (Φ_{fluo}) are computed according to

$$\Phi_{fluo} = k_r/(k_r + k_{nr}) \quad (5)$$

where k_r and k_{nr} are the radiative and the nonradiative decay rates from the emissive $\pi\pi^*$ state and are obtained with the TVCF formalism (see the formalisms in the Supporting Information). These calculations on **7** aim to explore if quantitative determinations of Φ_{fluo} can be fully attained from first principles (without the need of any experimental data), and they also serve us to benchmark our above-described computational protocol. These results are also reported in Table 2. First, the k_r obtained with the TVCF formalism (and thus through the explicit evaluation of the Franck−Condon-weighted density of states) is 1.2×10^8 sec^{-1}, and thus it is slightly larger than the one obtained with eq 3, that is, 7.3×10^7 sec^{-1}. Nevertheless, both values are of about the same order of magnitude, and we can conclude that, for these Schiff base complexes, the use of the more approximated eq 3 to compute the k_r values is adequate. The reorganization energy obtained through the TVCF formalism (2771 cm^{-1}) is also in accordance with the approximated amount through half of the computed Stokes shift (2523 cm^{-1}). All this evidence validates our chosen computational protocol for the rest of complexes. Finally, concerning the Φ_{fluo} value, the TVCF formalism predicts a smaller value than those obtained both experimentally and with eq 4, although it is in reasonable agreement with both of them. However, the fact that they are not directly comparable, since only the $\pi\pi^* \rightarrow S_0$ nonradiative deactivation is considered with the former approach, prevents us from extracting further conclusions.

In a nutshell, our investigations confirm the validity of the chelation-induced fluorescent enhancement effect for these Schiff base complexes. To attain larger photoluminescent efficiencies, the subtle choice of the central atom and the coordinating anion appears to be an optimal ingredient in the design of highly emissive Schiff base complexes, as it has a notable influence on the appearance of parasitic quenching processes (i.e., dark-state quenching and/or ISC processes).

DOI: 10.1021/acs.inorgchem.7b01692
Inorg. Chem. XXXX, XXX, XXX−XXX

5. CONCLUSIONS

Cadmium(II) and zinc(II) Schiff base complexes are cheap alternatives to 4d and 5d transition metal complexes for bioimaging and photonic applications. In this contribution we provide a deep insight into the photoluminescent properties of a series of Schiff base complexes of those two metal ions. Their photoluminescent properties are anion-dependent and are determined by a subtle competition between different photodeactivation channels. To unveil the origin of their different photoluminescent properties, computational investigations were performed. More in details, the PES of the complexes were explored, and quantitative determinations of their photoluminescence efficiencies from first-principles were obtained. The increased quantum yields of the Schiff base complexes as compared to the free ligands root on chelation-induced fluorescent enhancement effect. These investigations also evidence the subtle choice of the coordinating anion and the central metal atom to attain larger efficiencies. Finally, these studies should provide the ingredients for the optimal design of Schiff base complexes with tailored photoluminescence properties.

■ ASSOCIATED CONTENT

Supporting Information

The Supporting Information is available free of charge on the ACS Publications website at DOI: 10.1021/acs.inorgchem.7b01692.

Experimental details, X-ray data collection and crystal structure determination, Fourier transform infrared spectra, mass spectra, ^{1}H NMR spectra, UV−vis absorption spectra, TVCF formalisms, and numerical data of the TVCF calculations for complex **7** were provided (PDF)
CheckCIF/PLATON report (PDF)
CheckCIF/PLATON report (PDF)
CheckCIF/PLATON report (PDF)
CheckCIF/PLATON report (PDF)
CheckCIF/PLATON report (PDF)

Accession Codes

CCDC 1556526−1556530 contain the supplementary crystallographic data for this paper. These data can be obtained free of charge via www.ccdc.cam.ac.uk/data_request/cif, or by emailing data_request@ccdc.cam.ac.uk, or by contacting The Cambridge Crystallographic Data Centre, 12 Union Road, Cambridge CB2 1EZ, UK; fax: +44 1223 336033.

■ AUTHOR INFORMATION

Corresponding Authors

*E-mail: prateeti_17@yahoo.co.in. (P.C.)
*E-mail: Daniel.escudero@univ-nantes.fr. (D.E.)
*E-mail: dasdebasis2001@yahoo.com. (D.D.)

ORCID

Debasis Das: 0000-0003-4570-7168

Notes

The authors declare no competing financial interest.

■ ACKNOWLEDGMENTS

The authors wish to thank the Univ. of Calcutta for providing single-crystal X-ray diffractometer. X-ray diffractometer (under DST-FIST) and and the ESI-MS spectrophotometer from the DST PURSE. I.M. is thankful to UGC, India [UGC/689/Jr Fellow(Sc)(Up gradation)], for providing fellowship. D.E. is thankful for funding from the European Union's Horizon 2020 research and innovation programme under the Marie Sklodowska-Curie Grant No. 700961.

■ REFERENCES

(1) Cozzi, P. G. Metal−Salen Schiff base complexes in catalysis: practical aspects. *Chem. Soc. Rev.* **2004**, *33*, 410.
(2) O'Donnell, M. J. The Enantioselective Synthesis of r-Amino Acids by Phase-Transfer Catalysis with Achiral Schiff Base Esters. *Acc. Chem. Res.* **2004**, *37*, 506.
(3) Gupta, K. C.; Sutar, A. K. Catalytic activities of Schiff base transition metal complexes. *Coord. Chem. Rev.* **2008**, *252*, 1420.
(4) Nirmal, R.; Prakash, C. R.; Meenakshi, K.; Shanmugapandiyan, P. Synthesis and Pharmacological Evaluation of Novel Schiff Base Analogues of 3-(4-amino) Phenylimino) 5-fluoroindolin-2-one. *J. Young Pharm.* **2010**, *2*, 162.
(5) Valarmathy, G.; Subbalakshmi, R. Synthesis, Spectral Characterization and Biological Studies of Novel Schiff Base Complexes Derived from 4,6-dimethyl-2- sulfanilamidopyrimidine and 2-hydroxy-3-methoxybenzaldehyde. *Int. J. Pharm. Bio Sci.* **2013**, *4*, 287.
(6) Abuamer, K. M.; Maihub, A. A.; El-Ajaily, M. M.; Etorki, A. M.; Abou-Krisha, M. A.; Almagani, M. A. The Role of Aromatic Schiff Bases in the Dyes Techniques. *Int. J. Org. Chem.* **2014**, *4*, 7.
(7) Zyzak, D. V.; Sanders, R. A.; Stojanovic, M.; Tallmadge, D. H.; Eberhart, B. L.; Ewald, D. K.; Gruber, D. C.; Morsch, T. R.; Strothers, M. A.; Rizzi, G. P.; Villagran, M. D. Acrylamide Formation Mechanism in Heated Foods. *J. Agric. Food Chem.* **2003**, *51*, 4782.
(8) Jeevadason, A. W.; Murugavel, K. K.; Neelakantan, M. A. Review on Schiff bases and their metal complexes as organic photovoltaic materials. *Renewable Sustainable Energy Rev.* **2014**, *36*, 220.
(9) Yang, X.; Jones, R. A.; Huang, S. Luminescent 4f and d-4f polynuclear complexes and coordination polymers with flexible salen-type ligands. *Coord. Chem. Rev.* **2014**, *273−274*, 63.
(10) Barbieri, A.; Accorsi, G.; Armaroli, N. Luminescent complexes beyond the platinum group: the d^{10} avenue. *Chem. Commun.* **2008**, 2185.
(11) Zeng, H. H.; Thompson, R. B.; Maliwal, B. P.; Fones, G. R.; Moffett, J. W.; Fierke, C. Real-Time Determination of Picomolar Free Cu (II) in Seawater Using a Fluorescence-Based Fiber Optic Biosensor. *Anal. Chem.* **2003**, *75*, 6807.
(12) Yoon, J. Y.; Ohler, N. E.; Vance, D. L H.; Aumiller, W. D.; Czarnik, A. W. A fluorescent chemosensorsignalling only Hg(II) and Cu(II) in water. *Tetrahedron Lett.* **1997**, *38*, 3845.
(13) Kramer, R. Fluorescent Chemosensors for Cu^{2+} Ions: Fast, Selective, and Highly Sensitive. *Angew. Chem., Int. Ed.* **1998**, *37*, 772.
(14) Bernardo, M. A.; Pina, F.; Escuder, B.; Garcia-Espana, E.; Godino-Salido, M. L.; Latorre, J.; Luis, S. V.; Ramirez, J. A.; Soriano, C. Thermodynamic and fluorescence emission studies on chemosensors containing anthracene fluorophores. Crystal structure of $\{[CuL^1Cl]Cl\}_2 \cdot 2H_2O$ [L^1 = *N*-(3-aminopropyl)-*N*′-3-(anthracen-9-ylmethyl) aminopropylethane −1,2-diamine]. *J. Chem. Soc., Dalton Trans.* **1999**, 915.
(15) Darbha, G. K.; Singh, A. K.; Rai, U. S.; Yu, H.; Chandra Ray, P.; Yu, E. Selective Detection of Mercury (II) Ion Using Nonlinear Optical Properties of Gold Nanoparticles. *J. Am. Chem. Soc.* **2008**, *130*, 8038.
(16) Jiang, P.; Guo, Z. Fluorescent detection of zinc in biological systems: recent development on the design of chemosensors and biosensors. *Coord. Chem. Rev.* **2004**, *248*, 205.
(17) Kim, H. N.; Ren, W. X.; Kim, J. S.; Yoon, J. Fluorescent and colorimetric sensors for detection of lead, cadmium, and mercury ions. *Chem. Soc. Rev.* **2012**, *41*, 3210.
(18) Escudero, D.; Jacquemin, D. Computational insights into the photodeactivation dynamics of phosphors for OLEDs: a perspective. *Dalton Trans.* **2015**, *44*, 8346.

DOI: 10.1021/acs.inorgchem.7b01692
Inorg. Chem. XXXX, XXX, XXX−XXX

(19) Hrdlovic, P.; Donovalova, J.; Stankovicova, H.; Gaplovsky, A. Influence of Polarity of Solvents on the Spectral Properties of Biochromophoric Coumarins. *Molecules* **2010**, *15*, 8915.
(20) Lakowicz, J. R. *Principles of Fluorescence Spectroscopy,* 2nd ed.; Kluwer Academic Plenum Publishers: New York, 1999.
(21) Bevington, P. R. *Data Reduction and Error Analysis for the Physical Sciences;* McGraw Hill: New York, 1969; p 235.
(22) (a) *FELIX 32,* version 1.1; Photon Technology International, Inc.: Edison, NJ, 2003. (b) *FELIX GX,* version 2.0.1; Photon Technology International, Inc.: Edison, NJ, 2003.
(23) (a) SADABS Bruker AXS; *SAINT,* Software Users Guide,- Version 6.0; Bruker Analytical X-ray Systems: Madison, WI, **1999**. (b) Sheldrick, G. M. *SADABS,* v2.03: Area-Detector Absorption Correction. University of Göttingen: Germany, 1999.
(24) Altomare, A.; et al. *SIR97*: a new tool for crystal structure determination and refinement. *J. Appl. Crystallogr.* **1999**, *32*, 115.
(25) Sheldrick, G. M. *Acta Crystallogr., Sect. A: Found. Crystallogr.* **2008**, *A64*, 112.
(26) (a) Farrugia, L. J. *WinGX* and *ORTEP for Windows*: an update. *J. Appl. Crystallogr.* **2012**, *45*, 849. (b) van der Sluis, P.; Spek, A. L. BYPASS: an effective method for the refinement of crystal structures containing disordered solvent regions. *Acta Crystallogr., Sect. A: Found. Crystallogr.* **1990**, *46*, 194.
(27) (a) Shuai, Z. G.; Peng, Q.; Niu, Y. L.; Geng, H. *MOMAP, a free and open-source molecular materials property prediction package*, Revision 0.2.004; Shuai group: Beijing, China, 2014, http://www.shuaigroup.net/. (b) Peng, Q.; Yi, Y.; Shuai, Z.; Shao, J. Excited state radiationless decay process with Duschinsky rotation effect: Formalism and implementation. *J. Chem. Phys.* **2007**, *126*, 114302. (c) Peng, Q.; Yi, Y.; Shuai, Z.; Shao, J. Toward quantitative prediction of molecular fluorescence quantum efficiency: Role of Duschinsky rotation. *J. Am. Chem. Soc.* **2007**, *129*, 9333. (d) Niu, Y.; Peng, Q.; Shuai, Z. Promoting-mode free formalism for excited state radiationless decay process with Duschinsky rotation effect. *Sci. China, Ser. B: Chem.* **2008**, *51*, 1153. (e) Peng, Q.; Niu, Y.; Shi, Q.; Gao, X.; Shuai, Z. Correlation function formalism for triplet excited state decay: Combined spin−orbit and nonadiabatic couplings. *J. Chem. Theory Comput.* **2013**, *9*, 1132. (f) Shuai, Z. G.; Peng, Q. Excited states structure and processes: Understanding organic light-emitting diodes at the molecular level. *Phys. Rep.* **2014**, *537*, 123.
(28) Niu, Y.; Peng, Q.; Deng, C.; Gao, X.; Shuai, Z. Theory of Excited State Decays and Optical Spectra: Application to Polyatomic Molecules. *J. Phys. Chem. A* **2010**, *114*, 7817.
(29) Seybold, P. G.; Gouterman, M. Porphyrins: XIII: Fluorescence spectra and quantum yields. *J. Mol. Spectrosc.* **1969**, *31*, 1.
(30) Brook, D. J. R.; Fornell, S.; Stevens, J. E.; Noll, B.; Koch, T. H.; Eisfeld, W. Coordination Chemistry of Verdazyl Radicals: Group 12 Metal (Zn, Cd, Hg) Complexes of 1,4,5,6-Tetrahydro-2,4-dimethyl-6-(2′-pyridyl)-1,2,4,5-tetrazin-3(2*H*)-one ($pvdH_3$) and 1,5-Dimethyl-3-(2′-pyridyl)-6-oxoverdazyl (pvd). *Inorg. Chem.* **2000**, *39*, 562−567.
(31) Adhikary, J.; Chakraborty, P.; Samanta, S.; Zangrando, E.; Ghosh, S.; Das, D. Thiocyanate mediated structural diversity in phenol based "end-off" compartmental ligand complexes of group 12 metal ions: Studies on their photophysical properties and phosphatase like activity. *Spectrochim. Acta, Part A* **2017**, *178*, 114.
(32) Escudero, D. Revising Intramolecular Photoinduced Electron Transfer (PET) from First-Principles. *Acc. Chem. Res.* **2016**, *49*, 1816.
(33) Peng, Q.; Niu, Y.; Deng, C.; Shuai, Z. Vibration correlation function formalism of radiative and non-radiative rates for complex molecules. *Chem. Phys.* **2010**, *370*, 215.
(34) Shuai, Z.; Wang, D.; Peng, Q.; Geng, H. Computational Evaluation of Optoelectronic Properties for Organic/Carbon Materials. *Acc. Chem. Res.* **2014**, *47*, 3301.
(35) (a) Escudero, D. Quantitative prediction of photoluminescence quantum yields of phosphors from first principles. *Chem. Sci.* **2016**, *7*, 1262. (b) Peng, Q.; Shi, Q.; Niu, Y.; Yi, Y.; Sun, S.; Li, W.; Shuai, Z. Understanding the efficiency drooping of the deep blue organometallic phosphors: a computational study of radiative and non-radiative decay rates for triplets. *J. Mater. Chem. C* **2016**, *4*, 6829.

DOI: 10.1021/acs.inorgchem.7b01692
Inorg. Chem. XXXX, XXX, XXX−XXX